NUMERICAL ANALYSIS AND EXPERIMENTAL INVESTIGATION OF A TAIL ROTOR BLADE COMPOSITE TORSION.

Golovanov A.I., Mitryaykin V.I., Mikhaylov S.A., Konyukhov A.V.

Kazan Helicopter Joint Stock Association, Russia

INTRODUCTION.

One of the relevant problem concerning with helicopter load-bearing structure design is to supply static and dynamic stability of the structure. Difficulty of this problem increases if we consider elastic hingeless load-bearing elements of a helicopter rotor blade. Endurance supply is proportional to strength of mating structure elements. The investigation of more and more complex models is becoming state of the art of engineering practice.

Analytical methods, FEM, BEM and others allow to obtain results agreed with various mathematical models of solid mechanics, but final decision will be always given by the experiment. This paper deals with elastic hingeless load-bearing elements of the light helicopter rotor blade. The main difficulty of the structure analysis is that the element is not a part of the rotor, but a part of the blade. This element is used to transfer operating loads from the rotor to the blade. We called this element a "torsion". The torsion has multilayered structure and complex shape. In order to supply more durability, its shape has two transfer load ways. This structure is becoming state of the art in helicopter design and this one is implemented for the light helicopter "ANSAT". The main feature of the torsion structure is a multilayered composite structure with arbitrary shape. The torsion structure in transverse direction is a 17-19 layered package. Each layer, made of various materials (duralumin, glass-fiber material, rubber and etc.), has small thickness. Stiffness of one layer varies from the other in thousands times. It leads to a big error in stress evaluation if we use a multilayered element with thickness-average stiffness. That is why, 3D finite element method was chosen. Torsion structure was modeled as a multilayered package of finite elements. Two element types were considered. Both types have quadratic approximation along surface coordinates and linear one along normal.

In order to calculate strength-stress state and estimate durability of the torsion, numerical model has been developed and extensive experimental tests have been conducted.

This design is under development for the light helicopter "ANSAT" and tailored by Kazan Helicopter Joint Stock Association.

MATHEMATICAL MODEL.

Let us introduce the following notation. Strain vector in the global reference frame X,Y,Z is denoted as

$$\{\varepsilon\}^T = \{\varepsilon_{xx}, \varepsilon_{yy}, \varepsilon_{zz}, \gamma_{xy}, \gamma_{yz}, \gamma_{zx}\} \qquad (1)$$

and in the reference frame system associated with orthotropic direction α, β, γ as

$$\{\varepsilon_\alpha\}^T = \{\varepsilon_{\alpha\alpha}, \varepsilon_{\beta\beta}, \varepsilon_{\gamma\gamma}, \gamma_{\alpha\beta}, \gamma_{\beta\alpha}, \gamma_{\gamma\alpha}\}$$

and so does stress vector, consequently:

$$\{\sigma\}^T = \{\sigma_{xx}, \sigma_{yy}, \sigma_{zz}, \tau_{xy}, \tau_{yz}, \tau_{zx}\} \qquad (2)$$

$$\{\sigma_\alpha\}^T = \{\sigma_{\alpha\alpha}, \sigma_{\beta\beta}, \sigma_{\gamma\gamma}, \tau_{\alpha\beta}, \tau_{\beta\gamma}, \tau_{\gamma\alpha}\}$$

Hook's law can be written as

$$\{\sigma\} = [D]\{\varepsilon\}, \{\sigma_\alpha\} = [D_\alpha]\{\varepsilon_\alpha\}. \qquad (3)$$

Where

$$[D_\alpha] = \begin{bmatrix} d_{11} & d_{12} & d_{13} & 0 & 0 & 0 \\ d_{21} & d_{22} & d_{23} & 0 & 0 & 0 \\ d_{31} & d_{32} & d_{33} & 0 & 0 & 0 \\ 0 & 0 & 0 & G_{\alpha\beta} & 0 & 0 \\ 0 & 0 & 0 & 0 & G_{\beta\gamma} & 0 \\ 0 & 0 & 0 & 0 & 0 & G_{\gamma\alpha} \end{bmatrix}, \qquad (4)$$

$$d_{11} = \frac{1}{AE_\beta}\left(\frac{1}{E_\gamma} - \frac{\mu_{\beta\gamma}^2}{E_\beta}\right),\ d_{22} = \frac{1}{AE_\gamma}\left(\frac{1}{E_\alpha} - \frac{\mu_{\gamma\alpha}^2}{E_\gamma}\right),$$

$$d_{33} = \frac{1}{AE_\alpha}\left(\frac{1}{E_\beta} - \frac{\mu_{\alpha\beta}^2}{E_\alpha}\right),$$

$$d_{12} = d_{21} = \frac{1}{AE_\gamma}\left(\frac{\mu_{\gamma\alpha}\mu_{\beta\gamma}}{E_\beta} + \frac{\mu_{\alpha\beta}}{E_\alpha}\right),$$

$$d_{13} = d_{31} = \frac{1}{AE_\beta}\left(\frac{\mu_{\alpha\beta}\mu_{\beta\gamma}}{E_\alpha} + \frac{\mu_{\gamma\alpha}}{E_\gamma}\right),$$

$$d_{23} = d_{32} = \frac{1}{AE_\alpha}\left(\frac{\mu_{\alpha\beta}\mu_{\gamma\alpha}}{E_\gamma} + \frac{\mu_{\beta\gamma}}{E_\beta}\right),$$

$$A = \frac{1}{E_\alpha E_\beta E_\gamma}\left(1 - 2\mu_{\alpha\beta}\mu_{\beta\gamma}\mu_{\gamma\alpha} - \frac{E_\alpha}{E_\gamma}\mu_{\gamma\alpha}^2 - \frac{E_\beta}{E_\alpha}\mu_{\alpha\beta}^2 - \frac{E_\gamma}{E_\beta}\mu_{\beta\gamma}^2\right).$$

Let $[T]$ is a rotation matrix, that transforms X,Y,Z reference frame to α, β, γ reference frame associated with orthotropic directions. Assuming that, we can write strain in this reference frame as $\{\varepsilon_\alpha\} = [T]\{\varepsilon\}$. Elasticity matrix $[D]$ can be written as $[D] = [T]^T [D_\alpha][T]$.

Surface of the torsion has complex shape (cutouts, champfer and etc.), so we use quadratic displacement approximation. Number of layers are

high, but a layer thickness is small, so linear through the thickness displacement approximation is valid. Consider an element with linear through the thickness approximation and quadratic approximation for two surface coordinates. This is an 18-nodes element with quadratic approximation along surface coordinates ξ,η and linear approximation along thickness coordinate ς (Fig. 1).

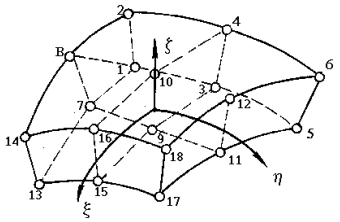

Fig. 1. 18-nodes element.

Dimensionless local coordinate system ξ,η,ς mapped each of elements described by X,Y,Z into simple cube ($-1\le\xi,\eta,\varsigma\le 1$) described by ξ,η,ς.

We introduce same shape functions $N_i(\xi,\eta,\varsigma)$ for both displacement vector $\{u,v,w\}$ and structure geometry.

$$\begin{cases} X(\xi,\eta,\varsigma)=\sum\limits_{i=1}^{18}x_iN_i(\xi,\eta,\varsigma),\\ Y(\xi,\eta,\varsigma)=\sum\limits_{i=1}^{18}y_iN_i(\xi,\eta,\varsigma),\\ Z(\xi,\eta,\varsigma)=\sum\limits_{i=1}^{18}z_iN_i(\xi,\eta,\varsigma), \end{cases}$$

$$\begin{cases} u(\xi,\eta,\varsigma)=\sum\limits_{i=1}^{18}u_iN_i(\xi,\eta,\varsigma),\\ v(\xi,\eta,\varsigma)=\sum\limits_{i=1}^{18}v_iN_i(\xi,\eta,\varsigma),\\ w(\xi,\eta,\varsigma)=\sum\limits_{i=1}^{18}w_iN_i(\xi,\eta,\varsigma), \end{cases}$$

Assuming that, Jacobian has form

$$[J]=\begin{bmatrix} \frac{\partial x}{\partial\xi} & \frac{\partial y}{\partial\xi} & \frac{\partial z}{\partial\xi}\\ \frac{\partial x}{\partial\eta} & \frac{\partial y}{\partial\eta} & \frac{\partial z}{\partial\eta}\\ \frac{\partial x}{\partial\varsigma} & \frac{\partial y}{\partial\varsigma} & \frac{\partial z}{\partial\varsigma} \end{bmatrix}=\sum_{i=1}^{18}\begin{bmatrix} x_i\frac{\partial N_i}{\partial\xi} & y_i\frac{\partial N_i}{\partial\xi} & z_i\frac{\partial N_i}{\partial\xi}\\ x_i\frac{\partial N_i}{\partial\eta} & y_i\frac{\partial N_i}{\partial\eta} & z_i\frac{\partial N_i}{\partial\eta}\\ x_i\frac{\partial N_i}{\partial\varsigma} & y_i\frac{\partial N_i}{\partial\varsigma} & z_i\frac{\partial N_i}{\partial\varsigma} \end{bmatrix}$$

and inverse Jacobi matrix has form $[C]=\left[J^{-1}\right]$.

After standard procedure we have expression for strain vector

$$\left\{\varepsilon^{6\times1}(\xi,\eta,\varsigma)\right\}=\sum_i\left[B_i^{6\times3}(\xi,\eta,\varsigma)\right]\begin{Bmatrix} u_i^{3\times1}\\ v_i\\ w_i \end{Bmatrix},$$

where derivatives shape function matrix has the following form

$$[B_i]=\begin{bmatrix} c_{11}\frac{\partial N_i}{\partial\xi}+c_{12}\frac{\partial N_i}{\partial\eta}+c_{13}\frac{\partial N_i}{\partial\varsigma} & 0 & 0\\ 0 & c_{21}\frac{\partial N_i}{\partial\xi}+c_{22}\frac{\partial N_i}{\partial\eta}+c_{23}\frac{\partial N_i}{\partial\varsigma} & 0\\ 0 & 0 & c_{31}\frac{\partial N_i}{\partial\xi}+c_{32}\frac{\partial N_i}{\partial\eta}+c_{33}\frac{\partial N_i}{\partial\varsigma}\\ c_{21}\frac{\partial N_i}{\partial\xi}+c_{22}\frac{\partial N_i}{\partial\eta}+c_{23}\frac{\partial N_i}{\partial\varsigma} & c_{11}\frac{\partial N_i}{\partial\xi}+c_{12}\frac{\partial N_i}{\partial\eta}+c_{13}\frac{\partial N_i}{\partial\varsigma} & 0\\ 0 & c_{31}\frac{\partial N_i}{\partial\xi}+c_{32}\frac{\partial N_i}{\partial\eta}+c_{33}\frac{\partial N_i}{\partial\varsigma} & c_{21}\frac{\partial N_i}{\partial\xi}+c_{22}\frac{\partial N_i}{\partial\eta}+c_{23}\frac{\partial N_i}{\partial\varsigma}\\ c_{31}\frac{\partial N_i}{\partial\xi}+c_{32}\frac{\partial N_i}{\partial\eta}+c_{33}\frac{\partial N_i}{\partial\varsigma} & 0 & c_{11}\frac{\partial N_i}{\partial\xi}+c_{12}\frac{\partial N_i}{\partial\eta}+c_{13}\frac{\partial N_i}{\partial\varsigma} \end{bmatrix}$$

Governing system in variational form can be written as

$$\begin{aligned} &\iiint\limits_v\left(\sigma_{xx}\delta\varepsilon_{xx}+\sigma_{yy}\delta\varepsilon_{yy}+\sigma_{zz}\delta\varepsilon_{zz}\right)dv+\\ &+\iiint\limits_v\left(\tau_{xy}\delta\gamma_{xy}+\tau_{yz}\delta\gamma_{yz}+\tau_{zx}\delta\gamma_{zx}\right)dv= \qquad (5)\\ &\iiint\limits_v\left(Q_x\delta u+Q_y\delta v+Q_z\delta w\right)dv+\iint\limits_{S_\sigma}\left(P_x\delta u+P_y\delta v+P_z\delta w\right)dS \end{aligned}$$

By Q_x,Q_y,Q_z we denote body loads, and by P_x,P_y,P_z surface loads. With these assumptions, left side of the equation (5) can be written as

$$\iiint\limits_v\{\sigma\}^T\{\delta\varepsilon\}dv=\iiint\limits_v\{\varepsilon\}^T[D]\{\delta\varepsilon\}dv=$$

$$=\sum_{i,j=1}^{18}\{u_i,v_i,w_i\}^T\iiint\limits_v[B_i]^T[D][B_j]dv\begin{Bmatrix}\delta u_j\\ \delta v_j\\ \delta w_j\end{Bmatrix}=$$

$$=\sum_{i,j=1}^{18}\{u_i,v_i,w_i\}^T\left[K_{ij}\right]\begin{Bmatrix}\delta u_j\\ \delta v_j\\ \delta w_j\end{Bmatrix},$$

where $\left[K_{ij}\right]$ is element stiffness matrix. Full dimension of stiffness matrix is 54×54.

Standard Gaussian quadrature is used to calculate element stiffness matrix. We take three points along surface direction and two points along transverse direction. Having known that $dv=\det[J]d\xi d\eta d\varsigma$, we write stiffness matrix as

$$\begin{aligned} \left[K_{ij}\right]&=\int_{-1}^{+1}\int_{-1}^{+1}\int_{-1}^{+1}[B_i(\xi,\eta,\varsigma)]^T[D][B_j(\xi,\eta,\varsigma)]\det[J(\xi,\eta,\varsigma)]d\xi d\eta d\varsigma=\\ &=\sum_{m,n=1}^{3}\sum_{k=1}^{2}[B_i(\xi_m,\eta_n,\varsigma_k)]^T[D][B_j(\xi_m,\eta_n,\varsigma_k)]\det[J(\xi_m,\eta_n,\varsigma_k)]\omega_m\omega_n\omega_k \end{aligned}$$

where ξ_m,η_n,ς_k are quadrature points and $\omega_m,\omega_n,\omega_k$ are weights.

If material properties are unsymmetrical along thickness we can't use elastic law in the form (3-4). Moreover, average out thickness stiffness leads to error in stress evaluation. Therefore, we introduce 3D layered element with various through the thickness material properties. This element analogous to shown in fig. 1, but it consists of layers and includes orthotropic material directions. Material properties of each layer may be orthotropic in the element plane. Let us denote α,β,γ are orthotropic material directions. We

assume that α,β plane is parallel to ξ,η coordinate surface, γ and ς directions are collinear (Fig. 2). In order to orient orthotropic directions we introduce vector $\bar{P}_1$ tangent to ξ and $\bar{P}_3$ normal to surface directions ξ,η. Thus, angle φ between $\bar{P}_1$ and α direction gives the orientation angle of orthotropic directions.

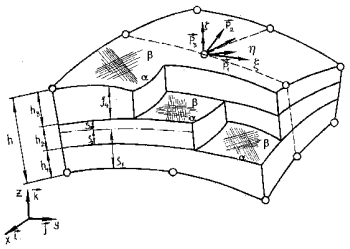

Figure 2. Multilayered finite element.

In order to calculate stiffness matrix we have to consider elasticity matrix $[D_\alpha]$ in the reference frame associated with orthotropic directions and elasticity matrix $[D]$ in the global reference frame X,Y,Z. Elasticity matrix $[D_\alpha]$ depends on $[D]$ with regard to rotation matrix $[T_\alpha]$.

$$T_\alpha=\begin{bmatrix} \cos^2\varphi & \sin^2\varphi & 0 & \sin\varphi\cos\varphi & 0 & 0 \\ \sin^2\varphi & \cos^2\varphi & 0 & -\sin\varphi\cos\varphi & 0 & 0 \\ 0 & 0 & 1 & 0 & 0 & 0 \\ 2\sin\varphi\cos\varphi & 2\sin\varphi\cos\varphi & 0 & \cos^2\varphi-\sin^2\varphi & 0 & 0 \\ 0 & 0 & 0 & 0 & \cos\varphi & -\sin\varphi \\ 0 & 0 & 0 & 0 & \sin\varphi & \cos\varphi \end{bmatrix}$$

If planar finite element has its α,β plane paralleled to X,Y plane we can write

$$[D]=[T_\alpha]^T[D_\alpha][T_\alpha]$$

We introduce "turning matrix" in case finite element has arbitrary nonplanar shape. This matrix transforms reference frame $\vec{i},\vec{j},\vec{k}$ into $\bar{P}_1,\bar{P}_2,\bar{P}_3$ and it has the following form:

$$[T_p]=\begin{bmatrix}[T_{11}] & [T_{12}] \\ [T_{21}] & [T_{22}]\end{bmatrix}$$

where

$$[T_{11}]=\begin{bmatrix} P_{1x}^2 & P_{1y}^2 & P_{1z}^2 \\ P_{2x}^2 & P_{2y}^2 & P_{2z}^2 \\ P_{3x}^2 & P_{3y}^2 & P_{3z}^2 \end{bmatrix}$$

$$[T_{12}]=\begin{bmatrix} P_{1x}P_{1y} & P_{1y}P_{1z} & P_{1z}P_{1x} \\ P_{2x}P_{2y} & P_{2y}P_{2z} & P_{2z}P_{2x} \\ P_{3x}P_{3y} & P_{3y}P_{3z} & P_{3z}P_{3x} \end{bmatrix}$$

$$[T_{21}]=\begin{bmatrix} 2P_{1x}P_{2x} & 2P_{1y}P_{2y} & 2P_{1z}P_{2z} \\ 2P_{2x}P_{3x} & 2P_{2y}P_{3y} & 2P_{2z}P_{3z} \\ 2P_{3x}P_{1x} & 2P_{3y}P_{1y} & 2P_{3z}P_{1z} \end{bmatrix}$$

$$[T_{22}]=\begin{bmatrix} (P_{1x}P_{2y}+P_{2x}P_{1y}) & (P_{1y}P_{2z}+P_{2y}P_{1z}) & (P_{1z}P_{2x}+P_{2z}P_{1x}) \\ (P_{2x}P_{3y}+P_{3x}P_{2y}) & (P_{2y}P_{3x}+P_{3y}P_{2z}) & (P_{2z}P_{3x}+P_{3z}P_{2x}) \\ (P_{3x}P_{1y}+P_{1x}P_{3y}) & (P_{3y}P_{1x}+P_{1y}P_{3z}) & (P_{3z}P_{1x}+P_{1z}P_{3x}) \end{bmatrix}$$

It needs two transformation if we want to evaluate strain in α,β,γ reference frame, because we have strain in X,Y,Z reference frame. The first transformation, given by matrix $[T_p]$, transforms reference frame X,Y,Z into $\bar{P},\bar{P}_2,\bar{P}_3$, the second one, given by $[T_\alpha]$, transforms $\bar{P}_1,\bar{P}_2,\bar{P}_3$ into α,β,γ. With these assumptions, elasticity matrix $[D]$ will be calculated as

$$[D]=[T_p]^T[T_\alpha]^T[D_\alpha][T_\alpha][T_p]$$

Displacements, strain and shape approximations, Jacobi matrix are still valid for this element type. The left part of the variation equation (5) will have the following form

$$\iiint_v\{\sigma\}^T\{\delta\varepsilon\}dv=\sum_{k=1}^{N}\iiint_{V_k}\{\varepsilon\}^T\left[D^{(k)}\right]\{\delta\varepsilon\}dv=$$

$$=\sum_{i,j=1}^{18}\{u_i,v_i,w_i\}^T\left[K_{ij}^{c'}\right]\begin{Bmatrix}\delta u_j\\ \delta v_j\\ \delta w_j\end{Bmatrix},$$

where $\left[D^{(k)}\right]$ is elasticity matrix for a layer with a number **k**. Matrix for one layer differs from the matrix for another layer due to various elasticity modulus or orientation angle φ. In order to integrate along ζ, we represent integral along package thickness as a sum of integrals along a layer thickness. Each of those integrals is calculated by one-point Gauss quadrature formulae. On this occasion we have

$$[K_{ij}]=\int_{-1}^{+1}\int_{-1}^{+1}\sum_{k=1}^{N}\int_{\varsigma_k}^{\varsigma_{k+1}}[B_i(\xi,\eta,\varsigma)]^T\left[D^{(k)}\right][B_j(\xi,\eta,\varsigma)]$$

$$\det[J(\xi,\eta,\varsigma)]d\xi d\eta d\varsigma=$$

$$=\sum_{m,n=1}^{3}\sum_{k=1}^{N}[B_i(\xi_m,\eta_n,\varsigma_k^*)]^T[B_j(\xi_m,\eta_n,\varsigma_k^*)]det[J(\xi_m,\eta_n,\varsigma_k^*)]2\Delta_k\omega_m\omega_n,$$

where $\varsigma_k^*=0{,}5(\varsigma_k+\varsigma_{k+1})$.

IMPLEMENTATION.

The numerical model, developed above, has been implemented to investigate stress-strength state in the tail rotor blade composite torsion of the light helicopter "ANSAT".

The torsion geometry model is 3D solid which has multilayered structure in transverse direction and complex shape in plane (fig. 3). Shape has five

holes and split into two transfer load ways by longitudinal cut.

The rotor shaft inserted into holes (1, 2). Small holes (3, 4) are served to transfer twisting loads for the helicopter control system. The spherical bearing of torsion hood inserted into the big hole (5).

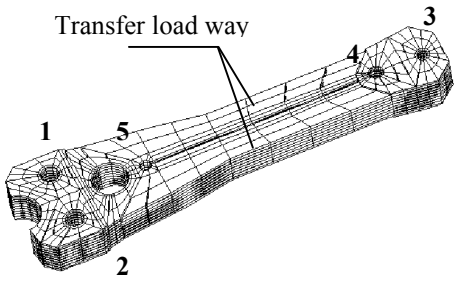

Figure 3. Finite element model of the torsion.

Material laying is nonuniform along thickness. Multilayered finite element was used for those layers, which had two layers of reinforcement fibers (reinforcement fibers directions are on the angle $\pm 45^0$). Ordinary element was used for other orthotropic layer.

Fig. 4 shows meshed model in X, У plane. Full dimension of the problem is 88746 degree of freedoms.

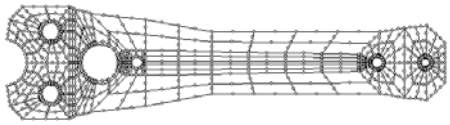

Figure 4. Front view of the torsion.

EXPERIMENTAL VERIFICATIONS.

In order to verify proposed numerical model, static tests of the torsion rotor blade were conducted. These experiments were provided by Research laboratory of A.N. Tupolev's Kazan Technical University (former Kazan Aircraft Institute) [2,3].

The test board consists of body tower, hydraulic jack, control and meter system. The left blade (to the rotation direction) is connected to swing bearing, the right blade is connected to hydraulic jack (Fig. 5).

Load has been applied to the rotor blade step by step. Magnitude of loads is determined by electronic extensionmeter. The MUP-100 test board together with KST-4 device provided calibration of the extensionmeter. Maximum error interval was within 2,4% level.

In order to measure magnitude of loads, deflections and strains, a computer system device has been used. It consisted of measure system SIIT-3, user interface and computer. Special software allowed calibrating each of the device channels before loading, and evaluating load magnitude, and measuring strains. Strain measurement is implemented by means of surface strain sensors, which were attached to external torsion surface. Figure 6 shows extensionmeter scheme. Even–numbered sensors were placed on lower surface and uneven-numbered ones were placed on upper surface.

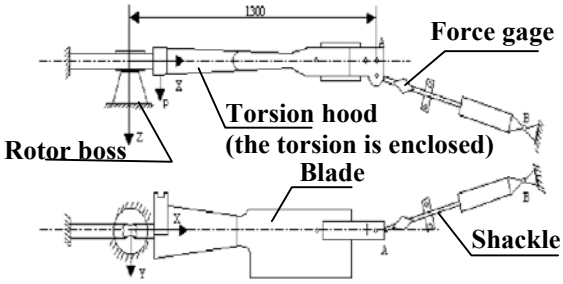

Figure 5. The test board scheme.

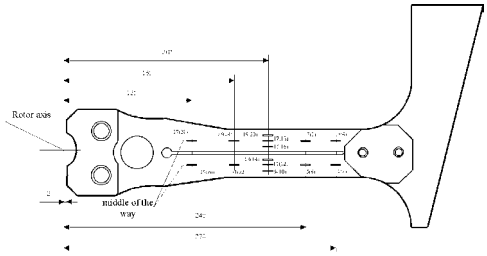

Figure 6. The extensionmeter scheme.

First, tests with simply loaded structure have been conducted in order to verify numerical results. After that a complex experiment was conducted in order to check various failure criterion.

Example 1.
Torsion loaded by axial force P_X =10000 N.

Symmetrically located sensors have various from each other results, so not only axial stress is nonzero, but also other stress. Therefore, complex stress state was realized in the test. This makes difficulty in verification process because of fact that only axial force has been applied in numerical evaluation. Meanwhile, as it is shown in table 1, (table 1 shows strains magnified in 10^6 times) maximum error in strain evaluation does not exceed 26% for most sensors. The worst case are located at section X =164 mm, nearby a torsion edge and nearby a hole for spherical bearing.

Example 2.
Bending of torsion in propulsion plane by force P_Z = -500 N.

Let us consider the torsion as a cantilever beam loaded by force at its end. We check out both vertical torsion displacements and strain.

Table 1.

Sensor number	Experiment	Numerical model		Sensor number	Experiment	Numerical model
1	162	210		15	169	160
2	163	210		16	181	160
3	149	210		17	273	247
4	157	210		18	287	247
5	195	215		19	374	272
6	171	215		20	401	272
7	285	215		21	296	228
8	309	215		22	228	228
9	179	272		23	218	228
10	175	272		24	311	228
11	157	247		25	111	184
12	187	247		26	241	184
13	132	160		27	112	184
14	153	160		28	244	184

Vertical displacements are measured by indication deflection gages symmetrically located along torsion ways. Table 2 shows coordinate of gages and experimental data as well. This experiment was repeated three times. We can see that data on a torsion way differs from that ones on the other torsion way. Therefore, not only bending stress state was realized, but also twist stress state. Figure 7 shows deflection curve. It is not as simple as it follows from the beam theory, it happened due to complex composite multilayered structure. Comparison between numerical and experimental data (fig. 8) shows good agreement and so does for strain (table 2).

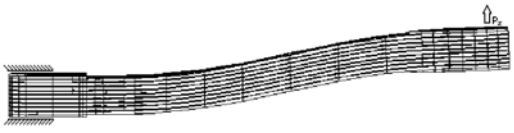

Figure 7. Deflection curve of the torsion.

Table 2.

Sensor number	Experiment	Numerical model		Sensor number	Experiment	Numerical model
1	51	48		15	24	21
2	50	48		16	-17	-21
3	-51	-48		17	29	32
4	49	48		18	-22	-32
5	-11	12		19	35	32
6	11	12		20	-27	-32
7	-12	-12		21	55	54
8	8	12		22	-55	-54
9	34	32		23	55	54
10	-29	-32		24	-55	-54
11	27	24		25	78	88
12	-23	-24		26	-75	-88
13	23	21		27	82	88
14	-18	-21		28	-79	-88

Figure 8.

Comparison between experimental and calculated deflection.

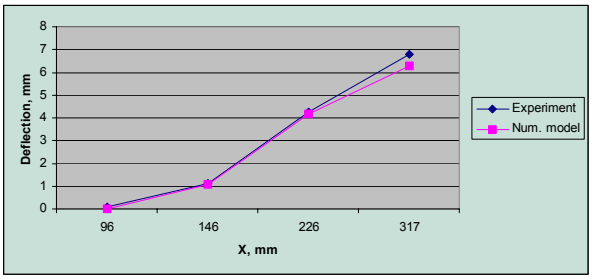

Example 3. Bending of a torsion in rotation plane by force P_X =500 N.

Table 3 shows experimental data in comparison with numerical ones. Disagreement between numerical and experimental results is about 32%. We see that tensile and squeeze zones are located on edge of the torsion, maximum strain is at the section X =165 mm.

Table 3.

Sensor number	Experiment	Numerical model		Sensor number	Experiment	Numerical model
1	-84	-75		15	10	33
2	-85	-75		16	34	33
3	113	75		17	76	98
4	46	75		18	91	98
5	-110	-84		19	143	123
6	-74	-84		20	157	123
7	84	84		21	-96	-106
8	103	84		22	-90	-106
9	-199	-123		23	53	106
10	-105	-123		24	103	106
11	-116	-98		25	-15	-39
12	-47	-98		26	-16	-39
13	-47	-33		27	-28	-39
14	10	33		28	37	39

STRESS-STRENGTH STATE OF THE TORSION.

Comparison between numerical results and experimental data shows that proposed numerical method allowes to calculate stress strength state in multilayered structures within engineering tolerance.

The next step in verification process is to investigate stress-strength state of the rotor blade torsion under actual loads. We consider the case named "Air puff". At this case there are nominal rotation of the aircrew together with turning of rotation plane and propulsion plane, as well as twisting of the torsion. Loads have been applied to the blade point at $X = 1{,}3$ m. in relation to rotor axis. Magnitudes of loads are $P_x = 128700$ N., $P_y = -990$ N., $P_z = 2620$ N. Wide range of loads leads to difficulty of controlling them during the experiment, therefore resultant of loads have been applied at the end of the blade. Together with these loads the rotor blade have been twisted at 10 degrees along longitudinal axis (from front edge to flange). The pretwisting has been obtained by special mechanism, which had allowed to control twisting angle of the rotor blade. Except these loading, the torsion had an additional twisting in that direction due to twisting load P_{twist}=307 N.

In order to apply loads on the blade, FEM model of the blade has been obtained. Finite element model of the blade has coarse mesh (it sufficient enough to apply loads), but finite element model of the torsion has very fine mesh. The conjunction technique, developed in [4], was used to connect the coarse meshed blade with the fine meshed torsion. This technique based on Lagrange multiplier method for governing variatonal equations. Lagrange multipliers regard as forces between conjunction parts. This implementation also allows parallel processing and can be effectively used for multiprocessor computers. The meshed model of the blade consists of three layers: facing layers and core. Facings made of fiber-glass material and core made of foam-composite. Figure 9 shows full meshed structure.

Macro criteria of strength and fracture of material have been used to estimate strength of the torsion. These criteria allow various failure mechanisms: fracture of tensile fibers, interfacial failure of adhesive, plastic failure of metal sheet [5]. As it known, there are many failure criteria, which include various damage mechanisms. Experiment proves that there are following typical ways of damage: fracture of tensile fibers in α or β directions and interfacial failure of adhesive. This leads to delamination or creep of fibers in tangent surface. We use a macrocriterion, which implies analytical dependence on stress.

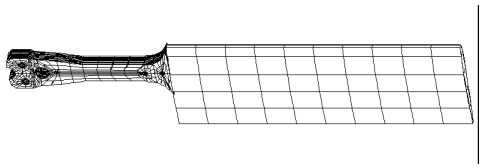

Figure 9. The blade-torsion structure.

Torsion design's features (namely, a high number of layers) and loads allow regarding each layer as a plane-stress state plate with stress σ_{xx}, σ_{yy}, τ_{xy}. Stress has discontinuity at the layer bound. Therefore, failure criterion, expressed in orthotropic directions stress $\sigma_{\alpha\alpha}$, $\sigma_{\beta\beta}$, $\tau_{\alpha\beta}$, is used for each layer respectively.

Improved model takes into account both shear stress $\tau_{\alpha\gamma}$, $\tau_{\beta\gamma}$ and squeeze thickness stress $\sigma_{\gamma\gamma}$. They can influence on strength state of middle package layers, which bore maximum level of the shear stress. In order to estimate delamination, interlaminar shear stress $\tau_{\alpha\gamma}$, $\tau_{\beta\gamma}$ are calculated.

If layer stress state close to plane stress state, we use the following criterion:

$$\frac{\sigma_{\alpha\alpha}^2}{\sigma_{\alpha}^{02}} + \frac{\sigma_{\beta\beta}^2}{\sigma_{\beta}^{02}} + \frac{\tau_{\alpha\beta}^2}{\tau_{\alpha\beta}^{02}} \le 1; \quad \begin{matrix} \sigma_{\alpha\alpha} \ge 0 \Rightarrow \sigma_{\alpha}^0 = \sigma_{\alpha}^{\mathrm{p}} \\ \sigma_{\alpha\alpha} < 0 \Rightarrow \sigma_{\alpha}^0 = \sigma_{\beta}^- \end{matrix};$$

$$\sigma_{\beta\beta} \ge 0 \Rightarrow \sigma_{\beta}^0 = \sigma_{\beta}^{\mathrm{p}}$$

$$\sigma_{\beta\beta} < 0 \Rightarrow \sigma_{\beta}^0 = \sigma_{\beta}^-$$

The criterion implies that yield surface is an individual ellipse in each quadrant of the stress space.

Next criterion is used for middle package layer, where there is an opportunity of appearance high level normal stress and shear stress.

$$\frac{\sigma_{\alpha\alpha}^2}{\sigma_{\alpha}^{\mathrm{p}}\sigma_{\alpha}^-} + \frac{\sigma_{\beta\beta}^2}{\sigma_{\beta}^{\mathrm{p}}\sigma_{\beta}^-} + \frac{\sigma_{\gamma\gamma}^2}{\sigma_{\gamma}^{\mathrm{p}}\sigma_{\gamma}^-} +$$

$$+ \frac{\tau_{\alpha\beta}^2}{\tau_{\alpha\beta}^{02}} + \frac{\tau_{\alpha\gamma}^2 + \tau_{\beta\gamma}^2}{\tau_{\alpha\gamma}^{02}} -$$

$$- \left(\frac{1}{\sigma_{\alpha}^{\mathrm{p}}\sigma_{\alpha}^-} + \frac{1}{\sigma_{\beta}^{\mathrm{p}}\sigma_{\beta}^-} - \frac{1}{\sigma_{\gamma}^{\mathrm{p}}\sigma_{\gamma}^-} \right) \sigma_{\alpha\alpha}\sigma_{\beta\beta} -$$

$$- \left(\frac{1}{\sigma_{\beta}^{\mathrm{p}}\sigma_{\beta}^-} + \frac{1}{\sigma_{\gamma}^{\mathrm{p}}\sigma_{\gamma}^-} - \frac{1}{\sigma_{\alpha}^{\mathrm{p}}\sigma_{\alpha}^-} \right) \sigma_{\beta\beta}\sigma_{\gamma\gamma} -$$

$$-\left(\frac{1}{\sigma_\gamma^{\mathrm{p}}\sigma_\gamma^-}+\frac{1}{\sigma_\alpha^{\mathrm{p}}\sigma_\alpha^-}-\frac{1}{\sigma_\beta^{\mathrm{p}}\sigma_\beta^-}\right)\sigma_{\gamma\gamma}\sigma_{\alpha\alpha}+$$

$$+\left(\frac{1}{\sigma_\alpha^{\mathrm{p}}}-\frac{1}{\sigma_\alpha^-}\right)\sigma_{\alpha\alpha}+\left(\frac{1}{\sigma_\beta^{\mathrm{p}}}-\frac{1}{\sigma_\beta^-}\right)\sigma_{\beta\beta}+$$

$$\times+\left(\frac{1}{\sigma_\gamma^{\mathrm{p}}}-\frac{1}{\sigma_\gamma^-}\right)\sigma_{\gamma\gamma}\le 1$$

The criterion implies that yield surface is a shifted ellipse in the stress space.

Those criteria include various damage mechanisms. It means that it is difficult to decide what type of damage happened if one of those criteria failed. In these cases, simple maximum stress criteria might be more effective. These relations can be expressed in form

$$-\sigma_\alpha^-\le\sigma_{\alpha\alpha}\le\sigma_\alpha^{\mathrm{p}};\ -\sigma_\beta^-\le\sigma_{\beta\beta}\le\sigma_\beta^{\mathrm{p}} \qquad (6)$$

$$\left|\tau_{\alpha\beta}\right|\le\tau_{\alpha\beta}^0 \qquad (7)$$

$$\left|\tau_{\alpha\gamma}\right|\le\tau_{\alpha\gamma}^0;\ \left|\tau_{\beta\gamma}\right|\le\tau_{\beta\gamma}^0;\quad -\sigma_\gamma^-\le\sigma_{\gamma\gamma}\le\sigma_\gamma^{\mathrm{p}} \qquad (8)$$

Brittle fiber failure in α or β would happen if the criterion (6) failed. Failure of adhesive and shear creep of fibers would happen if the criterion (7) failed. And at last, if the criterion (8) failed delamination would happen.

Thus, we suggest two step of stress-strength analysis. At the first step, we check if there are zones, where strength criterion failed. At the second step, by exploiting (6-8), we check what type of damage forms realized.

CONCLUSION.

As the results of investigation, it was revealed that there are zones where strength criterion failed (Fig. 10 shows stress intensity in upper surface layer). It is observed in the following layers: those layers which are close to the upper front face surface of bearing boss, those layers which are close to the blade (regions nearby rotor boss) and layers which have minimal thickness.

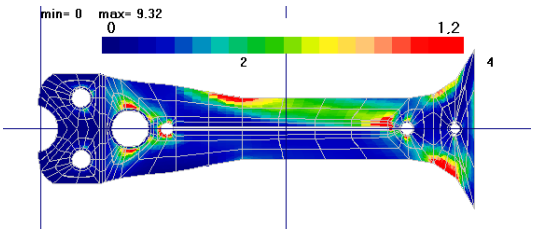

Figure 10.

Stress intensity in upper surface layer.

Detailed analysis, exploiting (6-8), shows that the main damage mechanism is brittle fiber failure in longitudinal and transverse direction. Experiment proved that mechanism.

ACKNOWLEDGEMENTS.

Kazan Helicopter Joint Stock Association has financed this research.

REFERENCES.

1. Obraztsov I.F., Savel'ev L.M., Khazanov Kh.S. Metod konechnyikh elementov v zadachah stroitel'noi mehaniki letatelnikh apparatov. [Finite element method in aircraft engineering. M.,: Vishaya shkola, 1985, 392 p.]
2. Bastrakov S.M. and others. Statichskie ispyitaniya obraztsa torsiona rulevoi lopasti experimentalnogo vertoleta "ANSAT". Otchet po NIR №1588 ONIL prochosti i nadezhnosti, KGTU, Kazan, 1998, 48 s. [Static tests of a tail rotor blade torsion specimen of the experimental helicopter "ANSAT", Reports of Research Laboratory №1588, Kazan State Technical University, Kazan, 1998, 48 p.]
3. Barbashev V.M. Technicheskaya sparvka po resultatam staticheskih ispyitaniy torsiona RV opyitnogo izdeliya ANSAT. KGTU, Kazan, 2000, 8s. [Technical guide on the result of static tests of the "ANSAT's" torsion. Kazan State Technical University, Kazan, 2000, 8 p.]
4. Golovanov A.I., Paymushin V.N. Dekonpozitsia sostavnyikh konstruktsyiy s nesopryazhennyimi setkami konechnyikh elementov na obschey grani i algoritm organizatsii parallelnyikh vyichisleniy// Prikladnyie problemyi prochnosti i plastichosti. N.Novgorod, 2000. – S.82-92. [Golovanov A.I., Paymushin V.N. Decomposition of complex structures meshed with nonconjugate mesh and algorithm of parallel solving//// Applied problems of the strength and plasticity. N.Novgorod, 2000. – P.82-92.]
5. Goldenblat I.I., Kopnev V.A. Kriterii prochnosti i plastichosti konstruktsionnyikh materialov. – M.: Mashinostroenoye, 1968. – 192 p. [Strength and plasticity criteria for structural material. – M.: Mashinostroenoye, 1968. – 192 p.].